DETONATION SPRAYING OF $AlCoCrFeNi_{2.1}$ EUTECTIC HIGH ENTROPY ALLOY COMPOSITE COATINGS REINFORCED BY Al_2O_3 PARTICLES

Ahmad Ostovari Moghaddam[1], Nataliya Shaburova[1], Dmitry Mikhailov[1], Kirill Pashkeev[1], Svetlana Trofimova[1], Denis Rybin[2], Marina Samodurova[1], Sergey Lezhnev[1], Evgeniy Panin[1], Evgeny Trofimov[1]

[1]South Ural State University, Chelyabinsk 454080
Russian Federation, ostovary@aut.ac.ir (A.O.M.); shaburovana@susu.ru (N.S.);
a_b_c81@mail.ru (D.M.); pashkeevki@susu.ru (K.P.);
trofmovasv7@gmail.com (S.T.); samodurovamn@susu.ru (M.S.);
sergey_legnev@mail.ru (S.L.); cooper802@mail.ru (E.P.); trofimovea@susu.ru (E.T.)
[2]Larentyev Institute of Hydrodynamics, Novosibirsk
630090, Russia, rybindenis1990@gmail.com (D.R.)

Received 20 November 2024
Accepted 14 January 2025
DOI: 10.59957/jctm.v60.i4.2025.13

ABSTRACT

$AlCoCrFeNi_{2.1}$ eutectic high entropy alloy (HEA) composite coatings reinforced by Al_2O_3 particles were prepared by detonation spraying (DS) on low alloy steel substrates. The effect of annealing at different temperatures on the microstructure and mechanical properties of the coatings was further studied. The as-deposited $AlCoCrFeNi_{2.1}$ - 30 wt. % Al_2O_3 composite coating exhibited a dual-phase FCC+BCC lamellar microstructure matrix with Al_2O_3 reinforcement particles. The crystalline structure and lamellar microstructure of the coatings highly retained after annealing at 500°C and 800°C. However, a partial dissolution of BCC was noted after annealing. Moreover, annealing improved inter-diffusion and annihilated pores, therefore highly compensated the decline in microhardness due to strain relief effect of annealing. The as-deposited composite exhibited a microhardness value of 415 HV, which slightly decreased to about 409 HV and 403 HV after annealing at 500°C and 800°C, respectively. The microhardness values demonstrated low fluctuation over the thickness of the coatings.

Keywords: *high entropy alloys, detonation spraying, lamellar microstructure, microhardness.*

INTRODUCTION

High entropy alloys (HEAs) are disordered crystalline solid solutions consisting of five or more elements with an equiatomic or nearly equiatomic ratio to maximize the configurational entropy of mixing [1]. HEAs are distinguished from conventional alloys by demonstrating high-entropy, lattice distortion, sluggish diffusion and cocktail effects as the four core effects. These effects provide HEAs with unprecedented properties such as the combination of high ductility and yield strength [2, 3], corrosion resistance [4], wear resistance [5], high-temperature oxidation resistance [6], and exceptional strength at low and high temperatures [7].

Recently Eutectic high-entropy alloys (EHEAs) were developed to utilize the characteristics of both eutectic alloys and HEAs, resolving the strength-ductility trade-off in conventional alloys. $AlCoCrFeNi_{2.1}$ is a typical EHEA exhibiting a dual-phase structure consisting of FCC and BCC/B2 phases. In its cast state, this alloy exhibits an average microhardness of ~320 HV and an elongation of 22.8 % at room temperature [8]. However, the alloy not yet met the criteria for working under harsh environments such as high loads, corrosion/wear resistance and high temperatures, suggesting further strengthening and improvement are inevitable.

Particularly, EHEAs can be employed as matrix and be reinforced by hard ceramic particles to further improve their mechanical properties. For example, AlCoCrFeNi HEA coating reinforced by WC was deposited on a 65Mn substrate using the laser cladding method to achieve a high microhardness value of 1060

$HV_{0.2}$ [9]. Ye et al. fabricated $AlCoCrFeNi_{2.1}$ EHEA reinforced with different TiC contents (0 - 15 wt. %) by micro-plasma cladding [10]. The decomposition of TiC was effectively reduced and the hardness and wear resistance of the coating significantly improved by TiC addition. Particularly, at 15 wt. % TiC, the coating showed the highest hardness and wear resistance. Wang et al. prepared AlCoCrFeNi composite reinforced by 0,5, 10, and 15 wt. % ZrB_2 by Spark Plasma Sintering (SPS). The composite exhibited a maximum densification of 99.13 % and microhardness of 1222.2 HV at ZrB_2 content of 15 %, white it shows the maximum compressive strength of 2071 MPa at 10 % ZrB_2. $AlCoCrFeNi_{2.1}$/WC composite coatings have been prepared by laser cladding and fast hot pressing sintering methods [11 - 13]. The laser cladded $AlCoCrFeNi_{2.1}$/WC composite coatings with 30 wt. % WC exhibited FCC and BCC phases along with the Cr_7C_3 and $Cr_{21}W_2C_6$ precipitates. The $AlCoCrFeNi_{2.1}$/30 wt. % WC composite coating exhibited the highest hardness (572.3 $HV_{1.0}$) and wear resistance. For the fast hot pressing sintering sample precipitation of W2C and $M_{23}C_6$ (M = W, Cr) was reported [13]. Solid solution, second-phase, and dislocation strengthening are typically the main strengthening mechanisms in these composites. Similar improvement in properties of $AlCoCrFeNi_{2.1}$ EHEA has been also noted by reinforcing the matrix with NbC [14].

On the other hand, detonation spraying (DS) is a thermal spraying technique, which is characterized by heating the particles up to the melting state and accelerating them to the velocity about 500 $m \cdot sec^{-1}$ with the help of the gaseous detonation energy [15]. The accelerated hot particles form a dense coating with the compressive or residual stress depending on the spraying conditions [16]. Typically, the DS fabricated coatings has strong mechanical bonding with the substrate and practically exhibit no heat-affected and diluted zones [17]. Therefore, DS can be a proper technique to deposit metal matrix composite (MMC) reinforced by hard ceramic particles.

To the best of the author's knowledge, there is no report on fabricating $AlCoCrFeNi_{2.1}/Al_2O_3$ composite coatings, and particularly no report on using DS for fabricating HEAs matrix coatings reinforced by ceramic particles. Therefore, in this study, $AlCoCrFeNi_{2.1}/Al_2O_3$ composite coatings were fabricated by DS and annealed at 500°C and 800°C. The effect of the Al_2O_3 and annealing on the microstructure and mechanical properties of the coating are investigated. The aim is to further expand the potential applications of $AlCoCrFeNi_{2.1}$ and reduce the materials cost for practical applications. This research also paves the way for fabricating new HEAs composite coatings using DS by incorporating high mass fraction of hard reinforcement particles.

EXPERIMENTAL

The $AlCoCrFeNi_{2.1}$ EHEA powder with spherical morphology and Al_2O_3 powders were purchased and used without any treatment. The $AlCoCrFeNi_{2.1}$ matrix composite powders were prepared by mixing 30 wt. % Al_2O_3 powder with the EHEA powder. A commercial detonation spraying gun CCDS2000 (Siberian Technologies of Protective Coatings LLC, Novosibirsk, Russia) was used for obtaining the composite coatings [18]. The spraying distance was set to 270 mm, feed rate was ~ 0.0375 g in shot (15 g in 400 shots), and the shots frequency was 2 shots per second. The explosive mixture of C_2H_2 / C_3H_8 /O_2 with ratio of oxygen to carbon (O/C) equal 1.0 (Chelyabtekhgaz, Chelyabinsk, Russia) was used for spraying and nitrogen was used as the purging and carrier gas.

X-ray diffraction (XRD) was carried out by a Rigaku Ultima IV X-ray diffractometer (Rigaku, Japan) using Cu-Kα radiation. Microstructural evolution and chemical composition were monitored by scanning electron microscope (SEM, Jeol JSM7001F, Japan) and energy dispersive X-ray spectroscopy (EDS; Oxford INCA X-max 80, Oxford Instruments, Great Britain), respectively. The average value of 5 measurements was used as the chemical composition at each location. Thixomet Pro software was used to evaluate the content of the porosity in the coatings.

RESULTS AND DISCUSSION

Fig. 1 shows the back scattered-electron SEM images of the powder's mixture feedstocks. The $AlCoCrFeNi_{2.1}$ EHEA powder exhibits spherical morphology with a size ranging from about 2 to 50 μm. The average particle size of $AlCoCrFeNi_{2.1}$ EHEA is about 23 μm (determined by ImageJ). Al_2O_3 exhibits an irregular grain morphology. The EDS elemental maps of the $AlCoCrFeNi_{2.1}$ EHEA indicate a uniform distribution

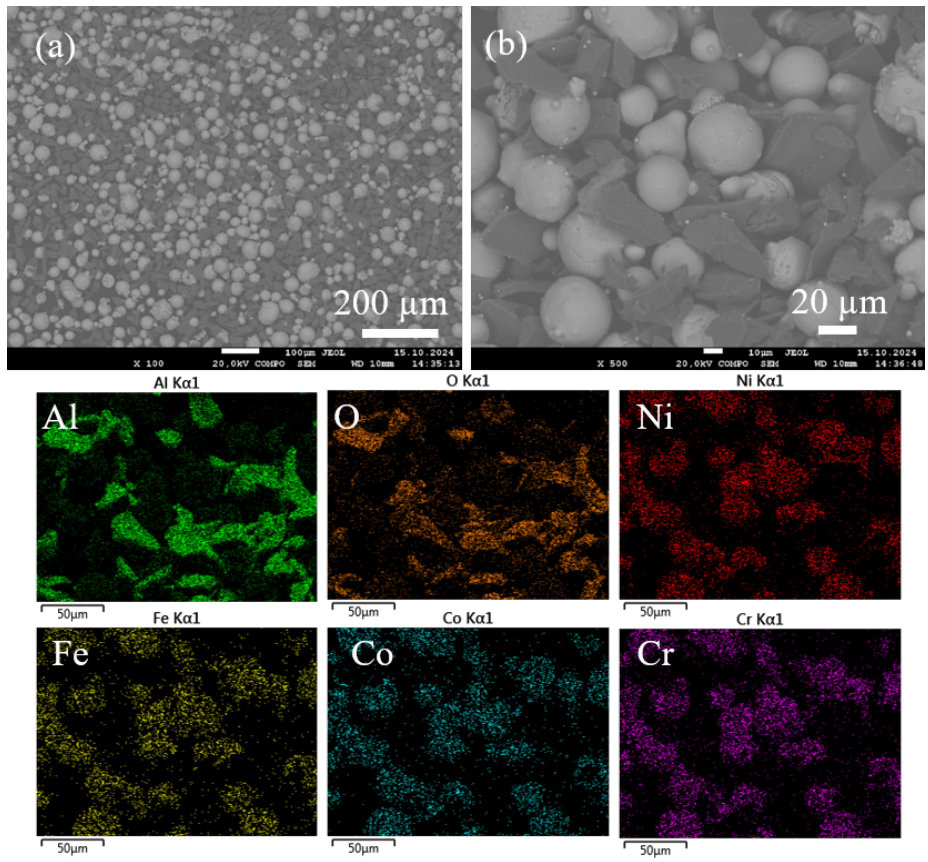

Fig. 1. BSE-SEM images and the corresponding maps of $AlCoCrFeNi_{2.1}/Al_2O_3$ mixture at low (a) and high (b) magnifications. The EDS maps belong to high magnification image in (b).

Table 1. Chemical composition of $AlCoCrFeNi_{2.1}/Al_2O_3$ composite coatings. The oxygen content should be treated qualitatively since EDS is not accurate for light elements.

EDS chemical composition, wt. %								
$AlCoCrFeNi_{2.1}$ powder	View type	Al	Cr	Co	Fe	Ni	O	Porosity, %
As-deposited coating	Bright contrast	18.41	16.61	16.04	15.65	33.29	-	~ 0.7
	Grey contrast	19.79	12.79	12.10	16.76	17.14	21.43	
	Dark contrast	37.91	1.60	1.27	1.28	2.40	55.54	
Annealed at 500°C	Bright contrast	16.82	17.22	16.11	16.31	33.55	-	~ 0.4
	Grey contrast	17.14	11.91	12.80	13.97	18.10	26.07	
	Dark contrast	40.63	0.99	1.00	1.05	1.82	54.50	
Annealed at 800°C	Bright contrast	7.78	18.78	19.65	18.48	35.30	-	< 0.1
	Grey contrast	27.83	14.47	14.00	13.03	17.51	13.16	
	Dark contrast	40.64	0.60	0.51	0.44	0.71	57.11	

of its constituent elements. Table 1 displays the chemical composition of the $AlCoCrFeNi_{2.1}$ EHEA.

Fig. 2 displays the XRD patterns of $AlCoCrFeNi_{2.1}/Al_2O_3$ powder mixture and the composite coatings at different states. The XRD pattern of the powder mixture can be well indexed with FCC, BCC and Al_2O_3 phases. It is obvious that the FCC and BCC structures attribute to the $AlCoCrFeNi_{2.1}$ EHEA. This is in agreement with previous studies where a FCC + BCC dual-phase structure has been reported for $AlCoCrFeNi_{2.1}$ EHEA

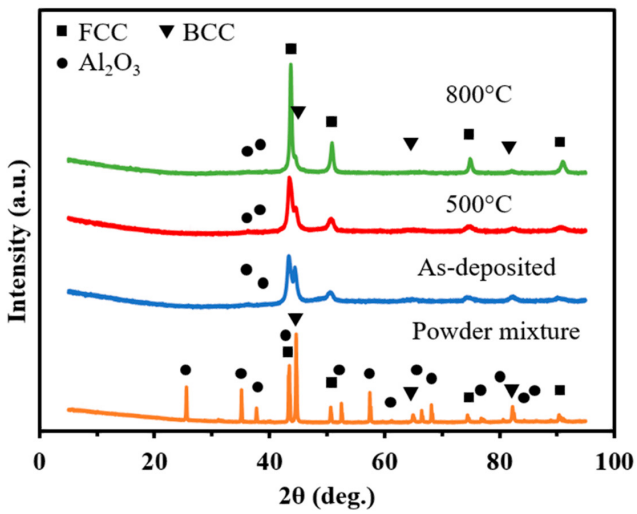

Fig. 2. XRD patterns of the $AlCoCrFeNi_{2.1}/Al_2O_3$ powder mixture, and the coatings in the as-deposited state and after annealing at 500°C and 800°C.

[19, 20]. After detonation spraying, diffraction peaks corresponding to FCC and BCC structures are still present in the XRD pattern of the as-deposited coating, however, diffraction peaks related to Al_2O_3 highly disappear but still can be detected. This decline in the intensity of diffraction peaks of Al_2O_3 may be ascribed to its refinement and dispersion within the matrix, as well as some degree of materials losses during DS. Moreover, a clear peak broadening can be detected in the XRD pattern, which indicates a relatively high level of residual strain and microstructure refinement during DS. After annealing at 500°C, the crystalline structure of the coating highly retained, but the relative intensity of BCC phase decreases. Furthermore, by increasing annealing temperature to 800°C, the BCC phase seems to be more dissolved and correspondingly the content of FCC phase increases. No specific changes in the diffraction peaks of Al_2O_3 by increasing annealing temperature can be noted. Interestingly, no other phases, especially oxides, form during DS owing to the short heating cycle of the process and high thermal stability of the powders. Typically, the short heating cycle involved in DS hinders interfacial reactions and phase decomposition in the as-sprayed coatings [21, 22].

BSE-SEM analysis was conducted to study the cross-section of the composite coatings. A thick coating with sound interface and dense microstructure is obtained by DS (Figs. 3a-b). Three different regions can be observed in the microstructure of the samples. The regions with bright contrast are Ni-rich FCC phase, while the grey contrast regions are Al- and Ni-rich BCC phase with an approximately equimolar ratio of other elements and some degree of oxidation (Table 1). This oxygen may come from Al_2O_3 or minor degree of oxidation during DS, which could not be detected by XRD due to its low content. The dark-contrast regions are rich in Al and oxygen, and they are obviously Al_2O_3 oxide. Moreover, the coatings exhibit a lamellar microstructure consisting of dark (Al_2O_3) and grey regions embedded within the bright regions (Fig. 3c). The high explosive temperature and wave force involved in DS technique make the HEA powder soft and readily deformable to create a continues matrix phase upon hitting the substrate surface. The Al_2O_3 particles, on the other hand, experience refinement and shattering during deposition owing to its hard nature. This creates a lamellar microstructure consisting of dual-phase HEA and Al_2O_3 layers. The thickness of the coating is about 700 µm. The microstructure is same across the thickness of the coatings without any sign of gradient features. EDS maps also confirm the presence of different microstructural features described above. Moreover, the composite coating demonstrates a rough interface with strong metallurgical bonding with the substrate.

Figs. 4a-b show the cross-sectional BSE-SEM micrographs of the coatings after annealing at 500°C and 800°C, respectively. For heat-treatment samples, coatings were made with a thickness of about 1000 µm to minimize the possible dilution of the coating by the substrate. Annealing does not change the microstructure significantly, and a still a lamellar microstructure is observed for both samples. However, the content of BCC phase (grey contrast regions) slightly decreased after annealing at 800°C, which is consistent with the XRD results. Moreover, annealing is expected to release the strain, annihilate pores and improve the metallurgical bonding between the coating and substrate by increasing inter-diffusion at the interface. The annealed coatings exhibit remarkable compactness with practically no detectable porosities. Moreover, the interface between $AlCoCrFeNi_{2.1}$ and Al_2O_3 is sound and stable, where no interfacial reactions could be detected. This suggests a good interfacial bonding and low detachment of Al_2O_3 reinforcement particles.

Microhardness of the samples was recorded on

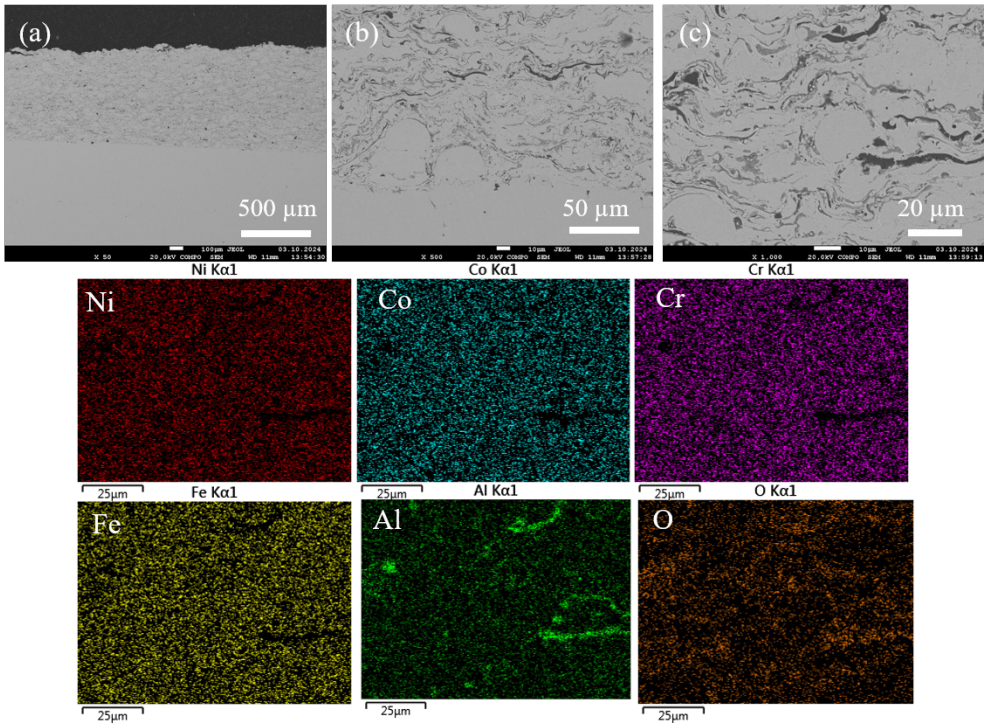

Fig. 3. BSE-SEM images and the corresponding maps of the as-deposited $AlCoCrFeNi_{2.1}/Al_2O_3$ composite coating at different magnification (a-c). The EDS maps belong to the high magnification image in (c).

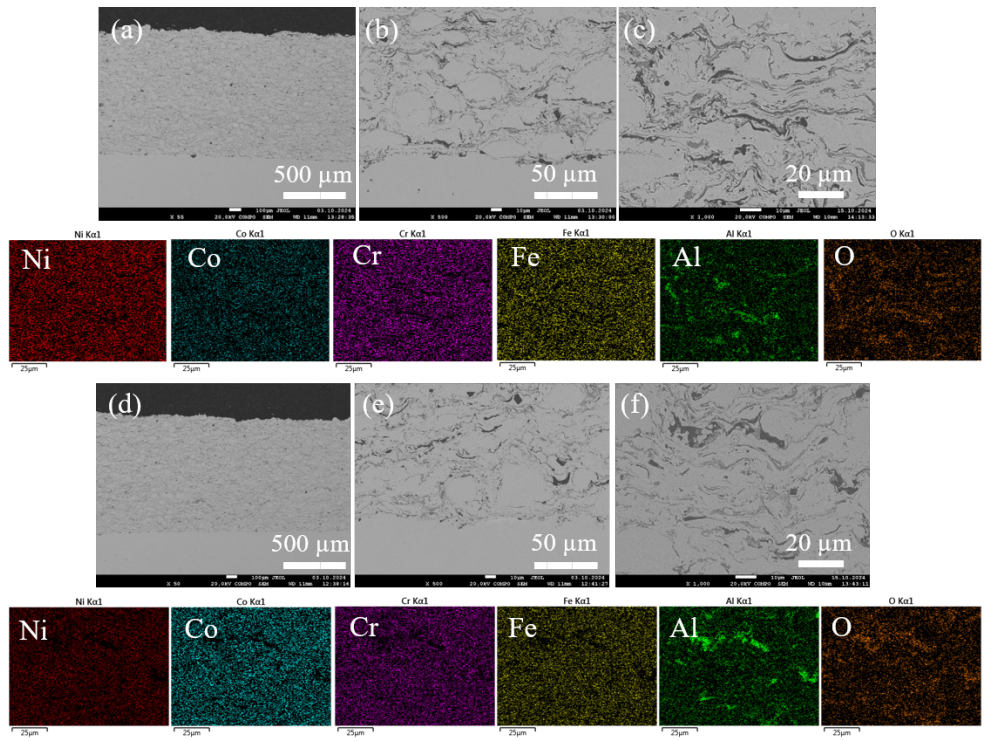

Fig. 4. BSE-SEM images and the corresponding maps of $AlCoCrFeNi_{2.1}/Al_2O_3$ composite coatings after annealing at 500°C (a-c) and 800°C (d-f). The EDS maps correspond to the high magnification images (c and f).

the cross-section of the composite coatings in a line parallel to the deposition direction (Fig. 5). The low alloy steel substrate shows a low hardness value of about 130 HV. After coating, the microhardness of the composite coatings increases even near the substrate-coating interface. The average microhardness of the $AlCoCrFeNi_{2.1}/Al_2O_3$ coating is 415 HV for the as-deposited sample, and it decreases to about 409 HV and 403 HV after annealing at 500°C and 800°C, respectively. Fig. 5 shows that the $AlCoCrFeNi_{2.1}/Al_2O_3$ composite coating highly retains its microhardness during high temperature annealing, where only a slight decrease can be noted.

This slight decrease in microhardness of the samples is due to strain release during annealing, given that the microstructure of the samples remains highly unaffected during annealing. Moreover, the microhardness values show no specific trend along the thickness of the composite coatings and change in a narrow range. This may be ascribed to the high uniform distribution of the reinforcing phases. Moreover, softening regions near coating/substrate that is usually detected in laser-cladded coatings is absent in the $AlCoCrFeNi_{2.1}/Al_2O_3$ composite coating fabricated by DS. This is a unique feature of DS compared to other coating methods where the substrate surface partially melts during coating deposition.

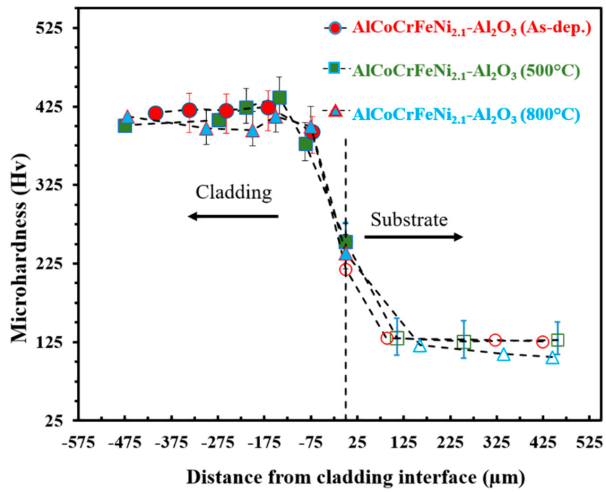

Fig. 5. Microhardness values measured along the coating thickness of $AlCoCrFeNi_{2.1}$ - 30 wt. % Al_2O_3 composite coatings in the as-deposited and annealed states.

CONCLUSIONS

$AlCoCrFeNi_{2.1}$ - 30 wt. % Al_2O_3 composite coating was fabricated by detonation spraying followed by annealing at 500°C and 800°C. The $AlCoCrFeNi_{2.1}$ - 30 wt. % Al_2O_3 composite precursor powder was mixed. AlCoCrFeNi2.1 EHEA exhibited a dual-phase microstructure consisted of FCC and BCC phases. After detonation spraying, diffraction peaks related to Al_2O_3 appeared, however the intensity of peaks decreased compared to the as-mixed powders, which could be attributed to the particle refinement, dispersion and some degree of materials losses during DS. After annealing at 500°C and 800°C, the crystalline structure of the coating highly retained, but BCC phase in HEA dissolved and correspondingly the content of FCC phase increased. Moreover, the coatings exhibited sound interface and dense lamellar microstructure consisting of Al_2O_3 and BCC phases embedded within the FCC matrix. It was also demonstrated that annealing does not alter the microstructure of the coatings, and the lamellar microstructure is retained. The average microhardness of the as-deposited composite coating was 415 HV, and it slightly decreased to about 409 HV and 403 HV after annealing at 500°C and 800°C, respectively. This highly retained mechanical properties of the coating is attributed to the improved inter-diffusion and annihilation of pores, as well as the unique properties of HEA matrix.

Acknowledgements

The study was funded by a grant from the Russian Science Foundation № 20-19-00304. https://rscf.ru/en/project/20-19-00304/

Authors contributions: *A. O. M. - conceptualization, methodology, investigation, writing - original draft; N. Sh. - investigation, writing - original draft, resources; D. M. - investigation, writing - original draft, validation; K. P. - investigation, visualization, validation; S. T. - investigation, data curation; D. R. - resources, software; M. S. - conceptualization, methodology, funding acquisition, writing - review and editing, project administration; S. L. - formal analysis, software; E. P. - visualization, formal analysis; E. T. - conceptualization, methodology, investigation, writing - original draft, validation.*

REFERENCES

1. A. Ostovari Moghaddam, R. Fereidonnejad, M. Naseri, N. Shaburova, S. Taskaev, S. Uporov, D. Mikhailov, A.H. Lashkari, E. Trofimov, Synthesis and Characterization of Nanocrystalline High Entropy Heusler Intermetallics Powders, Metals and Materials International, 30, 2024, 1424-1429. https://doi.org/10.1007/s12540-023-01573-w
2. J. Gong, W. Lu, Y. Li, S. Liang, Y. Wang, Z. Chen, A single-phase $Nb_{25}Ti_{35}V_5Zr_{35}$ refractory high-entropy alloy with excellent strength-ductility synergy, Journal of Alloys and Compounds, 1006, 2024, 176290. https://doi.org/10.1016/j.jallcom.2024.176290
3. S. Wang, Z. Chen, R. Chen, Z. Wu, Y. Jia, W. Zhang, Y. Wang, W. Liu, Y. Zhao, R. Shi, B Cao, S. Yu, Superior strength-ductility synergy in additively manufactured CoCrFeNi high-entropy alloys with multi-scale hierarchical microstructure, Journal of Alloys and Compounds, 1006, 2024, 176268. https://doi.org/10.1016/j.jallcom.2024.176268
4. J. Liu, Z. Lv, Z. Wu, J. Zhang, C. Zheng, C. Chen, D. Ju, L. Che, Research progress on the influence of alloying elements on the corrosion resistance of high-entropy alloys, Journal of Alloys and Compounds, 1002, 2024, 175394. https://doi.org/10.1016/j.jallcom.2024.175394
5. X. You, T. Li, J. Song, Y. Du, H. Wang, P. Lin, W. Zhou, Y. Zhang, L. Hu, A systematic study on wear behavior of TiCrNbTaWx refractory high-entropy alloy: Inducing amorphization to achieve anti-wear, Tribology International, 201, 2025, 110208. https://doi.org/10.1016/j.triboint.2024.110208
6. O. Samoilova, I. Suleymanova, N. Shaburova, A. Ostovari Moghaddam, E. Trofimov, The Behavior of $Al_{0.5}CoCrFeNiCuPt_{0.3}$ High-Entropy Alloy During High-Temperature Oxidation, High Temperature Corrosion of Materials, 101, 2024, 811-825. https://doi.org/10.1007/s11085-024-10248-9
7. Y. Zhou, J. Zhang, J. Zhang, X. Yao, J. Luan, Q. Li, S. Liu, B. Xiao, J. Ju, S. Zhao, Y. Zhao, Z. Sun, A strong-yet-ductile high-entropy alloy in a broad temperature range from cryogenic to elevated temperatures, Acta Materialia, 268, 2024, 119770. https://doi.org/10.1016/j.actamat.2024.119770
8. Y. Lu, Y. Dong, H. Jiang, Z. Wang, Z. Cao, S. Guo, T. Wang, T. Li, P.K. Liaw, Promising properties and future trend of eutectic high entropy alloys, Scripta Materialia, 187, 2020, 202-209. https://doi.org/10.1016/j.scriptamat.2020.06.022
9. L. Xu, M. Li, Z. Song, F. Li, J. Guo, M. Gao, WC-High Entropy Alloy Reinforced Long Life Self-Grinding Silage Knife Prepared by Laser Cladding, Nanomaterials, 12, 2022, 1013. https://doi.org/10.3390/nano12061013
10. F. Ye, Y. Yang, Z. Lou, L. Feng, L. Guo, J. Yu, Microstructure and wear resistance of TiC reinforced $AlCoCrFeNi_{2.1}$ eutectic high entropy alloy layer fabricated by micro-plasma cladding, Materials Letters, 284, 2021, 128859. https://doi.org/10.1016/j.matlet.2020.128859
11. Z. Li, D. Xie, F. Lv, K. Zhou, C. Jiao, X. Gao, D. Wang, Y. Liu, H. Zu, L. Shen, Effect of WC on the microstructure and mechanical properties of laser-clad $AlCoCrFeNi_{2.1}$ eutectic high-entropy alloy composite coatings, Journal of Alloys and Compounds, 976, 2024, 173219. https://doi.org/10.1016/j.jallcom.2023.173219
12. Y. Li, Y. Yu, J. Wang, Q. Yu, N. Tan, G. Zhang, J. Qi, Y. Yin, Y. Cai, Effect of WC content on the microstructure and properties of $AlCoCrFeNi_{2.1}$ eutectic high entropy alloy coating prepared by ultra-high speed laser cladding technology, Materials Today Communications, 41, 2024, 110259. https://doi.org/10.1016/j.mtcomm.2024.110259
13. B. Liu, H. Chen, J. Zhou, W. Wang, S. Xi, X. Chen, Interfacial bonding behavior of WC/$AlCoCrFeNi_{2.1}$ eutectic high-entropy alloy matrix composites fabricated by fast hot pressing sintering, Vacuum, 217, 2023, 112574. https://doi.org/10.1016/j.vacuum.2023.112574
14. H. Jiang, L. Li, J. Wang, C. Wei, Q. Zhang, C. Su, H. Sui, Wear Properties of Spark Plasma-Sintered $AlCoCrFeNi_{2.1}$ Eutectic High Entropy Alloy with NbC Additions, Acta Metallurgica Sinica (English Letters), 36, 2023, 987-998. https://doi.org/10.1007/s40195-023-01529-4
15. V. Ulianitsky, A. Shtertser, S. Zlobin, I. Smurov, Computer-Controlled Detonation Spraying: From Process Fundamentals Toward Advanced Applications, Journal of Thermal Spray Technology, 20, 2011, 791-801. https://doi.org/10.1007/s11666-011-9649-6

16. V.Yu. Ulianitsky, I.S. Batraev, D.K. Rybin, D.V. Dudina, A.A. Shtertser, A.V. Ukhina, Detonation Spraying of Cr_3C_2-NiCr Coatings and Their Properties, Journal of Thermal Spray Technology, 31, 2022, 598-608. https://doi.org/10.1007/s11666-021-01301-z
17. Ostovari Moghaddam, M. Sudarikov, N. Shaburova, M. Polyakova, M. Samodurova, E. Trofimov, Microstructural Evolution of High-Entropy Intermetallic Compounds during Detonation Spraying, Metals, 14, 2023, 50. https://doi.org/10.3390/met14010050
18. V.Y. Ulianitsky, D.V. Dudina, A.A. Shtertser, I. Smurov, Computer-controlled detonation spraying: Flexible control of the coating chemistry and microstructure, Metals, 9, 2019, 1244, https://doi.org/10.3390/met9121244
19. P. Peng, X. Feng, S. Li, B. Wei, M. Zhang, Y. Xu, X. Zhang, Z. Ma, J. Wang, Effect of heat treatment on microstructure and mechanical properties of as-cast $AlCoCrFeNi_{2.1}$ eutectic high entropy alloy, Journal of Alloys and Compounds 939, 2023, 168843. https://doi.org/10.1016/j.jallcom.2023.168843
20. X.-Y. Tian, H.-L. Zhang, Z.-S. Nong, X. Cui, Z.-H. Gu, T. Liu, H.-M. Li, E. Arzikulov, Effect of Alloying on Microstructure and Mechanical Properties of $AlCoCrFeNi_{2.1}$ Eutectic High-Entropy Alloy, Materials, 17, 2024, 4471. https://doi.org/10.3390/ma17184471
21. A.O. Moghaddam, N. Shaburova, M. Naseri, Y. Latfulina, M. Samodurova, V. Krymsky, K. Litvinyuk, E. Trofimov, Detonation Spraying of Ni-Based Composite Coatings Reinforced by High-Entropy Intermetallic Particles, Metals, 13, 2023, 1807. https://doi.org/10.3390/met13111807
22. G. Huang, L. Li, J. Cheng, W. Chen, J. Chen, S. Zhu, J. Yang, Tribological behavior of detonation sprayed $CrFeNiAl_{0.3}Ti_{0.3}$ high entropy alloy coatings in seawater environment, Tribology International, 194, 2024, 109480. https://doi.org/10.1016/j.triboint.2024.109480